Eccentricity strongly modulates visual processing delays

Johannes Burge[1,2,3,*] & Callista M. Dyer[1]

[1.]Department of Psychology, University of Pennsylvania, Pennsylvania PA
[2.]Neuroscience Graduate Group, University of Pennsylvania, Pennsylvania PA
[3.]Bioengineering Graduate Group, University of Pennsylvania, Pennsylvania PA
[*]Correspondence to jburge@upenn.edu

Abstract
The temporal dynamics of visual information processing varies with the stimulus being processed and with the retinal location that initiates the processing. Here, we present psychophysical data with sub-millisecond resolution showing that visual eccentricity strongly impacts the delay with which stimuli are processed. Even within the central +/-6º of the visual field, we show that processing delays change by up to a factor of approximately three. A simple model, grounded in how retinal physiology changes with eccentricity, provides a quantitative account of the data with one free parameter. The relative delays are on the order of only milliseconds. But if later processing leaves them unresolved, dramatic misperceptions of motion and 3D layout can result. We discuss the implications for how the human visual system solves the temporal binding problem across eccentricity. The results highlight the severe computational challenge of obtaining accurate, temporally-unified percepts of the environment with temporally-staggered processing across the visual field.

Acknowledgments
The authors have no conflicts of interest to disclose. This work was supported by NIH grant R01-EY028571 from the National Eye Institute & Office of Behavioral and Social Science Research to J.B.. The authors thank Kathryn Bonnen for helpful discussion and Nicolas Cottaris for generous assistance with the ISETBIO software package.

Keywords
periphery, binocular disparity, blur, 3D orientation

Introduction

Catching a ball at dusk is more difficult than at high noon. Starting with the photoreceptors, visual processing is slower when overall light-levels are low (Lit, 1949; Baylor & Hodgkin, 1973; Drum, 1984; Sinha et al., 2017; Burge et al., 2019). When the sensory periphery signals the rest of the nervous system with more delay, there is less time to react. The temporal dynamics of visual processing depend on many stimulus properties other than overall light-level. Different contrasts (Nachmias, 1967; Reynaud & Hess, 2017), colors (Cottaris & DeValois, 1998), level of detail (i.e. spatial frequency) (Harkness & Levi, 1979; Min et al., 2021; Chin & Burge, 2022), and levels of image sharpness (Burge et al., 2019; Rodriguez-Lopez et al., 2020; Rodriguez-Lopez et al., 2023) are all processed with different temporal dynamics (e.g. delays and temporal blurring). In any natural image, these stimulus properties tend to vary substantially across the visual field. The sky may be bright, blue, and devoid of detail; the underbrush may be dark, green, and full of detail. So neural signals carrying information about each location of a given image will tend to move through the early stages of the visual system in a temporally staggered fashion. However, it is largely unknown how visual field location modulates the speed with which any given stimulus property is processed.

Here, we ask how visual field location *itself* modulates the speed with which a given stimulus property is processed. We develop a paradigm that provides measurements of visual processing delays with sub-millisecond resolution, enabling precise characterization of how processing speed changes with eccentricity. The eccentricity at which a given stimulus property is processed strongly modulates the speed of visual processing (Carrasco et al., 2003).

To probe peripheral regions of the visual field, subjects binocularly viewed a rotating annulus of white circular beads for 250ms, with unequal retinal illuminance in the two eyes (Fig. 1AB). Such a stimulus undergoing rotational motion in the frontal plane will be perceived as pitched back. (The image in the darker eye is processed milliseconds more slowly.) We use this stimulus in a psychophysical experiment to measure a discrepancy in processing speed between the eyes. Then, we examine how this interocular delay changes as a function of eccentricity. Our data suggests, with measurements having sub-millisecond precision, that different eccentricities within the central $\pm 6^{\circ}$ of the visual field are processed with location-dependent delays that differ by over three times.

This stimulus presentation protocol takes advantage of a well-known stereo-motion-in-depth illusion known as the Pulfrich effect (Pulfrich,1922; Lit, 1949). When a horizontally oscillating target in the frontal plane is viewed with unequal retinal illuminance in the two eyes, the target is inaccurately perceived as moving along a near-elliptical trajectory in depth. The illusory motion in depth occurs because the image in the eye with lower illuminance is processed more slowly. (It has more recently been shown that interocular differences in contrast (Reynaud & Hess, 2017), blur (Burge et al., 2019; Rodriguez et al., 2020), spatial frequency (Chin & Burge, 2022), and color (Chin & Burge, in prep) can also cause the classic Pulfrich effect and its variants.) For moving targets, the difference in processing speed causes a neural disparity, which leads to the misperception of motion.

Relatively little is known about how the speed of visual processing changes across the visual field. Temporal sensitivity, the smallest temporal modulation that is just detectable, provides a measure of how much the visual system blurs a signal in time, and is well-known to increase with eccentricity (Kelly, 1984): the flicker fusion frequency, for example, is higher in the periphery than in central vision. (This is why fluorescent lights in badly lit bars can sometimes be seen to flicker from the corner of one's eye.) Comparatively little is known about how temporal delay—differences in processing speeds—, a measure of location in time, changes across the visual field.

Few studies have examined the question (Carrasco et al., 2003; Jovanovic & Mammasian, 2020). Fewer still contain within-subjects measurements having the temporal precision required to measure the computations at the time-scale at which they unfold. Despite the fact that the temporal dynamics of visual processing depend on the stimulus and its location in the visual field, percepts tend to be accurate and temporally unified. Rigidly moving scenes, for example, tend to be perceived as moving rigidly. The present findings challenge vision science to develop a rigorous understanding of how temporally staggered signals caused by the same event are bound in time.

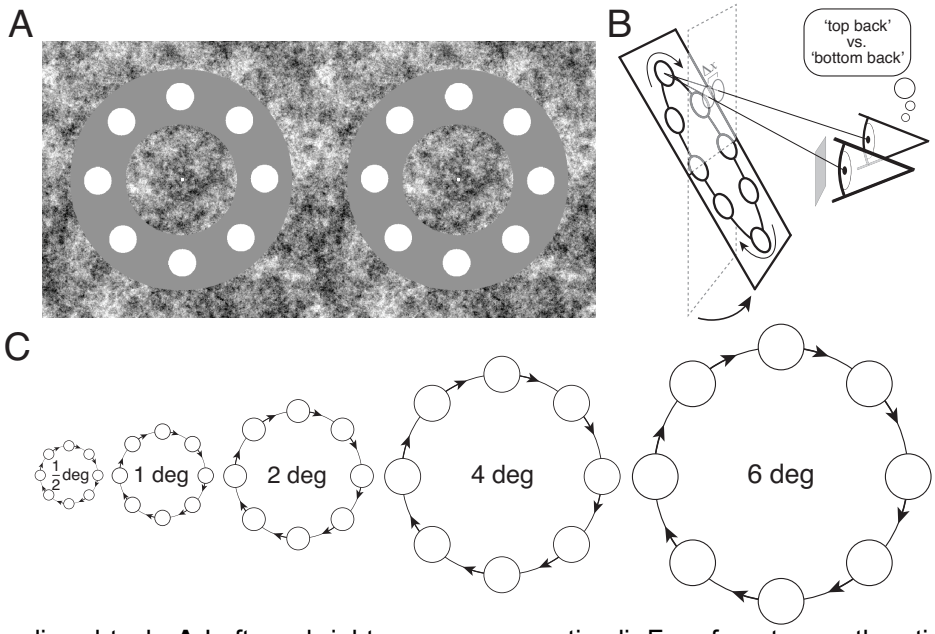

Figure 1. Stimuli and task. **A** Left- and right-eye onscreen stimuli. Free-fuse to see the stimuli in depth. Divergent-fusing will produce a 'top-back' percept. Cross-fusing will produce a 'bottom-back' percept. **B** If the left eye receives less light than the right eye, the left-eye image will be processed with more delay. With moving stimuli, a neural disparity will occur, and the beads will be perceived as rotated 'top back' with respect to the screen. The effective neural disparity at a given bead location Δx is given by the product of the horizontal velocity component v_x of the bead motion, and the interocular neural delay Δt, assuming that onscreen delays are zero. The critical onscreen delay was that which nulled the neural delay, and made the beads appear to rotate in the plane of the screen. **C** Critical onscreen delays were measured for a range of visual eccentricities. The onscreen delay that is required to null the perceived rotation out of the plane of the screen has the same magnitude but opposite sign of the neural delay. Circular bead sizes (10, 20, 40, 80, 120arcmin) and rotational speeds (1, 2, 4, 8, 12deg/sec) grew in proportion to eccentricity.

RESULTS AND DISCUSSION

Psychophysical Results

Main Experiment

To measure the eccentricity-dependent delays in the human visual system, we designed a one-interval two-alternative forced-choice (2AFC) experiment. The stimulus was a rotating set of circular beads that followed the center of an annulus-shaped 'racetrack' (Fig. 1AB). On each trial, for 250ms, the beads rotated either clockwise or counter-clockwise while the subject fixated a central dot. A haploscope enabled dichoptic stimulus presentation. Interocular luminance differences were introduced programmatically. The interocular luminance differences causes either one eye's image to be processed with more delay than the other. This interocular delay, in turn, causes the set of beads to be perceived as moving in a plane different than the screen plane. The task was to report, on each trial, whether the plane in which the beads were moving appeared

to be pitched ‘top-back’ or ‘bottom-back’ (Fig. 1B). For a given interocular luminance difference and eccentricity, there is a critical onscreen delay that caused the beads to be perceived as moving in the plane of the screen. The aim of the experiments was to find this critical onscreen delay.

On each trial, onscreen interocular delay was chosen in pseudo-random fashion. If onscreen-delay was zero, the onscreen binocular disparities on each frame specified that the beads were rotating in the plane of the screen (see Methods). If the onscreen-delay was non-zero, onscreen binocular disparities specified that the plane in which the beads were rotating was pitched top-back or bottom-back relative to the screen plane (Fig. 1B). In each condition, we computed the proportion of trails in which subjects responded ‘top-back’ as a function of onscreen interocular delay. Data was collected for four interocular luminance differences—which we express as interocular optical density differences (ΔO)—and at each of five eccentricities. Different eccentricities were probed by changing the radius of the annulus-shaped racetrack (Fig. 1C).

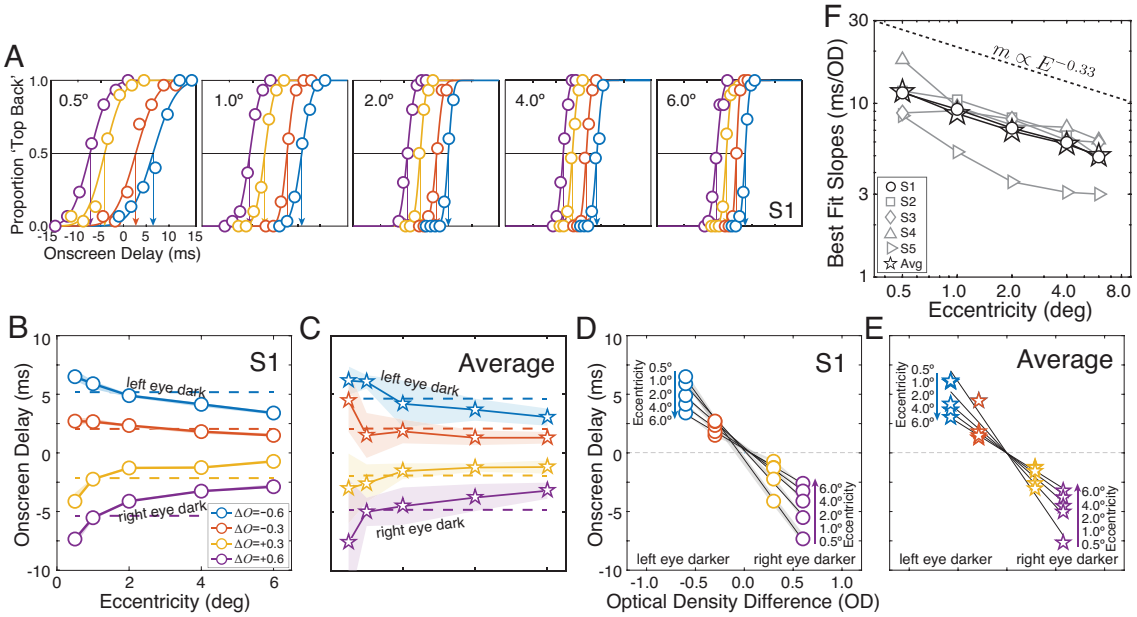

Figure 2. Main experiment. A Psychometric functions for the first human subject. Proportion ‘top back’ chosen as a function of onscreen delay for each luminance difference (colors) and each eccentricity (subplots) for subject S1. **B** Critical onscreen delay as a function of eccentricity for four interocular luminance differences (colors; ΔO=[-0.6,-0.3,0.3,0.6]). Delays decrease systematically with eccentricity. Shaded regions indicate bootstrapped 68% confidence intervals (approximately ±1 standard error). In cases where shaded regions are not visible, it is because the confidence interval is smaller than the datapoint. **C** As in B, but for averaged data across subjects (see Methods). Shaded regions indicate standard deviations across subjects. **D** Interocular delays as a function of interocular difference in optical density, for five different eccentricities (replotted data in A). Best-fit regression lines, computed via weighted linear regression, are also shown. The slopes of the best-fit lines decrease systematically with eccentricity, again indicating that the same luminance difference causes smaller interocular delays as eccentricity decreases. **E** As in D, for averaged subject data. **F** Best-fit slopes (see C and E) at each eccentricity for all individual subjects and the average data (symbols and solid lines). The best-fit power function—computed from the average data (stars)—is also shown (dashed black line). A given interocular luminance difference causes delays that are proportional to eccentricity raised to a power of -1/3. This result entails that an 8-fold increase in eccentricity will be associated with 2-fold decrease in visual processing delay.

The psychometric functions for the first human subject are shown in Fig. 2A. The functions get closer together as eccentricity increases, indicating that a fixed interocular luminance difference

has less effect on processing delays in the visual periphery. (The psychometric functions also get steeper with eccentricity. This result indicates that delay discrimination thresholds are smaller in the periphery, a finding consistent with their being better temporal contrast sensitivity (e.g. higher flicker fusion frequencies) in the visual periphery (Kelly, 1984); see Supplement Fig. S1). We summarize performance by computing the point of subjective equality (PSE). The PSE is the onscreen interocular delay corresponding to the 50% point on the psychometric function (colored arrows). The PSE specifies the critical onscreen delay that is required to null the neural disparity and make the beads appear to rotate in the plane of the screen. The critical onscreen delays should thus be equal in magnitude, and opposite in sign, to the neural delays in each condition.

Critical onscreen delays decrease systematically with eccentricity (Fig. 2B). For each of four different luminance differences (colors), as eccentricity increases from 0.5º to 6.0º (panels), the interocular delay decreases by ~2.5x. For example, when the right eye received 75% less light than the left (ΔO=+0.6) the amount by which the left-eye image had to be delayed onscreen decreased from 7.3ms near the fovea (0.5º of eccentricity) to only 2.9ms in the near periphery (6.0º of eccentricity). The data averaged across subjects follows a similar pattern as the data from the first individual subject (Fig. 2C). (Data from each of the five individual subjects show approximately the same pattern; see Supplementary Fig. S2.) Replotting the data in Fig. 2BC reveals that the critical onscreen delays change linearly with optical density difference (ΔO), and that the best-fit lines (see Methods) have slopes that decrease systematically with eccentricity (Fig. 2DE). (This eccentricity-dependent decrease in the slopes is reflected in the psychometric functions by how they get closer together as eccentricity increases; see Fig. 2A.)

A convenient way to summarize the influence of eccentricity on visual processing delays (while minimizing the effect of measurement error), is to plot how the slopes of the best-fit lines in Fig. 2BD change with eccentricity. Figure 2F shows, for each of the five human subjects and the subject average, the decrease in processing delay associated with a proportional increase in eccentricity. The proportional (and absolute) changes in processing delay with eccentricity are largely similar across different individuals. The data is well described by a power function (i.e. a line on a log-log plot) of the form $m=E^p$ over the range of tested eccentricities. A power of p=-0.33 provides the best fit both to data from the first human subject (see Fig. 2BC) and to the averaged subject data (see Fig. 2DE). Hence, for a given interocular luminance difference, an 8-fold increase in eccentricity entails a 2-fold decrease in visual processing delay.

Size-Control Experiment

Well-designed scientific studies attempt to rule out obvious potential confounding factors as alternative explanations of the results (Burge & Burge, 2022). The stimuli in the main experiment were composed of beads with sizes that covaried (i.e. scaled perfectly with) with the eccentricity being probed (see Fig. 1C). But stimulus size itself has been identified as a factor that can modulate the temporal properties of visual processing, both in psychophysics and neurophysiology (Virsu et al., 1982; Watson, 1986; Carrasco et al., 2003; Dacey et al., 2000; Bair, Cavanaugh, Movshon, 2003; Churan, Richard, Pack, 2009). To justifiably conclude that eccentricity is the principal determinant of the effects reported here, bead size must therefore be controlled for.

We conducted a size-control experiment that was identical to the original experiment, except that bead-size was held constant at all eccentricities (Fig. 3A). If the data from the control experiment are the same as those from the original experiment, the change in bead-size with eccentricity can be ruled out as an explanation of the results. Data from the size-control and original experiments are shown in Fig. 3B (left and right subplots, respectively). Clearly, the patterns are quite similar:

the changes in critical onscreen delay from 1.0º to 6.0º of eccentricity in the control experiment are nearly identical to the changes in the initial experiment.

To more rigorously compare the data, after subtracting off the effect of luminance differences, we plotted how critical onscreen delay changed with eccentricity in the two experiments against each other. We then computed the correlation and best-fit slope (Fig. 3BC). (Failing to regress out the effect of luminance differences would artificially inflate the correlation and distort the slopes.) For the first human subject, the data from the two experiments are essentially identical. The correlation between the change in delays was high and significant (ρ=0.97, p=5.6x10^{-10}). Perhaps more importantly, the slope of the best-fit line is not significantly different than 1.0 (m=0.91, CI^{95}=[0.78 1.07]), the slope one would expect if bead-size had no influence on the results. Similar patterns of results are obtained for the averaged subject data (Fig. 3DE; see Supplementary Fig. S2 for all individual subject data.) The control experiment shows that, in this task, bead-size changes do not alter visual processing delays. Bead-size, therefore, is not confounding the results.

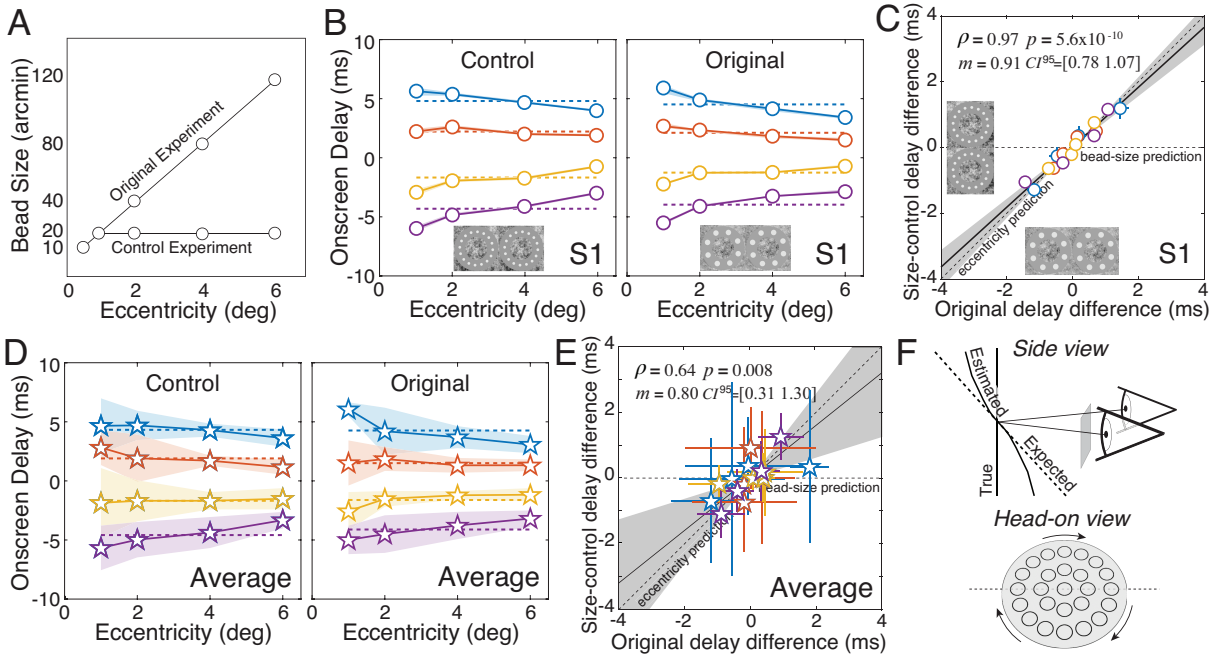

Figure 3. Size-control experiment. A In the original experiment, bead size increased in proportion to eccentricity. In the control experiment, bead size was held constant at all eccentricities. **B** Critical onscreen delays as a function of eccentricity at each luminance difference (colors) in both the control experiment (left) and the original experiment (right) for the first human subject. Note that eccentricity-dependent biases are removed so that the change in delay with eccentricity is more readily apparent. **C** Data from the control experiment plotted against data from the original experiment for the first human subject, after regressing out average delays due to luminance differences (dashed lines in B). The eccentricity-dependent changes in critical onscreen delay were significantly correlated between the two experiments (ρ=0.97, p=5.6x10^{-10}). The best-fit slope, obtained using Deming regression, was not significantly different from 1.0 (m=0.91, CI^{95}=[0.78 1.07]). Shaded regions show 95% confidence intervals on the best-fit slopes obtained from 1000 bootstrapped datasets. We conclude that bead-size had no measurable effect on processing delay. **D** As in B but with data averaged across all five subjects in the experiment. Shaded regions indicate the standard deviation across subjects in each condition. **E** As in C, but for data averaged across all subjects. The correlation between the data in the two experiments is clear and significant (ρ=0.64, p=0.008), and the best-fit slope is not significantly different from 1.0 (m=0.80, CI^{95}=[0.31 1.30]). The evidence indicates that bead-size has no significant effect on delay. **F** Perceptual consequences of eccentricity-dependent delays for a binocularly viewed spinning object.

What are the potential consequences of these eccentricity-dependent processing delays for visual perception? Consider a pepperoni pizza, viewed in lighting conditions like those in this experiment, that has been tossed into the air and is spinning on its axis. If later processing leaves the eccentricity-dependent delays unresolved, striking perceptual errors will result. For the situation depicted in Fig. 3F, the flat pizza will be seen to have a S-shape. But this particular perceptual illusion does not typically occur. Others illusions of this sort, that would be predicted from the stereo-geometry given spatially-variant temporal processing, do not typically occur. Rigidly moving objects typically appear rigid. For the many temporally staggered signals from the sensory periphery to contribute to a coherent unified percept, they must eventually be bound together in time. An important direction for future research is to develop an understanding of how these temporal-binding mechanisms work, and under what circumstances they fail.

Model from retinal physiology

Why does eccentricity impact visual processing delays? More specifically, why does a given luminance difference induce larger delays in the central than in the peripheral visual field? Here, we ask whether the manner in which basic properties of the retina change with eccentricity can account for the processing delays that we have measured psychophysically.

We pursue this line of inquiry because the classic Pulfrich effect is widely thought to have its origins in the processing of the retina itself (Prestrude & Baker, 1968; Prestrude, 1971; Rogers & Anstis, 1972; Mansfield & Daugman, 1978; Lennie, 1981; Bolz, Rosner, Wassle, 1982; Wolpert et al., 1993; see below for evidence supporting this consensus view). However, the Pulfrich effect has not previously been measured in the visual periphery. So, although a great deal is known about how various aspects of retinal physiology change with eccentricity, it is not known whether the effects reported here can be accounted for by how the temporal properties of response change across the retinal surface.

To investigate, we built a simple model. The model incorporates how three major facets of retinal physiology change with eccentricity: photoreceptor inner-segment diameters increase, photoreceptor outer-segment lengths decrease, and macular pigment density decreases (Curcio et al., 1990; Banks et al., 1991; Putnam & Bland, 2014; Cottaris et al., 2019) (Fig. 4A). Consistent with measurements of cone phototransduction (Sinha, 2022; Baudin, Angueyra, Sinha, Rieke, 2019), the model also assumes that, for a given light-adapted state at a moderate photopic light-level in line with our experimental conditions (~100cd/m^2), i) each photoreceptor must catch a threshold number of photons before a response is elicited, and ii) that this threshold number of photons does not change within the central $\pm$20° of the visual field.

If peripheral cone photoreceptors absorb more photons per unit time—that is, have a higher photon 'catch rate'—than foveal cone photoreceptors, perhaps the decrease in delay with eccentricity is straightforwardly accounted for. In line with available data, we assume that photon catch rate scales proportionally to i) the area of the inner-segments, ii) the length of the outer-segments (because longer outer-segments contain more opsin molecules and hence absorb a greater proportion of incident photons), and iii) the transmittance of the macular pigment. The scale factors relating these factors to photon catch rate are taken from the literature (Cottaris et al., 2019), and were implemented via the Image Systems Engineering Toolbox for Biology software package (ISETBio, http://isetbio.org).

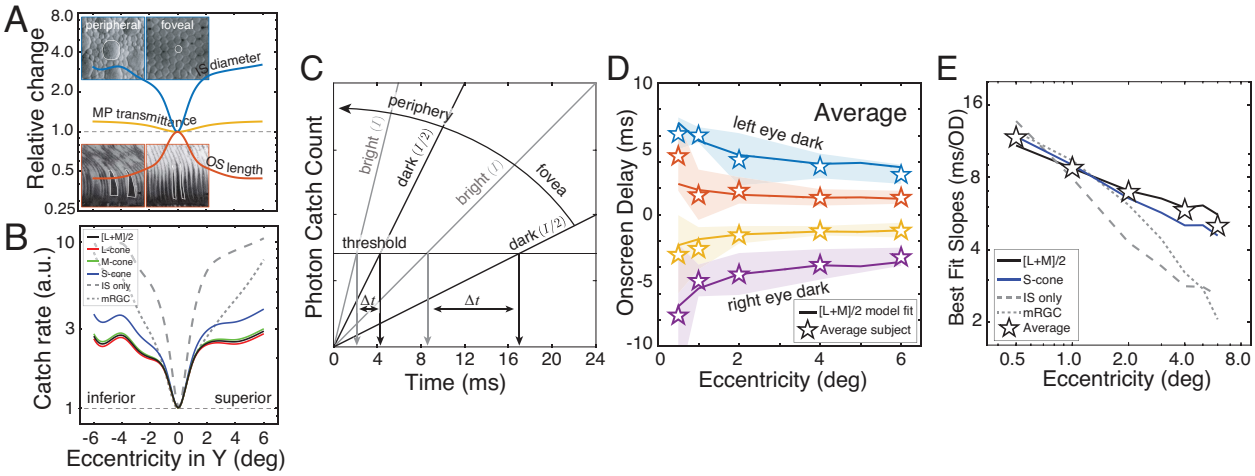

Figure 4. Retinal physiology-based model predictions. **A** Changes in retinal physiology with eccentricity, expressed as proportional change relative to the fovea. Cone inner-segment (IS) diameters increase (blue), cone outer-segment (OS) lengths decrease (red), and macular pigment transmittance (yellow) increases with eccentricity. Insets (adapted from Curcio et al., 1990) show peripheral and foveal cone IS diameters (top) and cone OS lengths (bottom), with individual examples outlined in white. **B** Photon catch rate, expressed as proportional change relative to the fovea, based on differences shown in A, for the L-, M-, and S-cones. The cone-specific catch rates differ because of how the cone spectral sensitivities interact with the spectral transmittance of the macular pigment, which passes less light in the short- than in the long-wavelength portion of the spectrum. Also shown are catch rates for the inner-segments only and for the midget ganglion cells (mRGCs). **C** Visualization showing how interocular delays (Δt) are predicted from catch rates (slopes) for a 2-fold difference in light intensity(I) between the eyes. Higher catch rates in the periphery (see B) predict smaller interocular delays than in the fovea. **D** Model fit (solid curves) to average subject data (stars) for all eccentricities and luminance differences. The model uses the mean catch rate of L- and M-cone catch rate (i.e. [L+M]/2). A single free-parameter—the threshold number of photons—was used to fit the data across all conditions. Changing the threshold value multiplicatively scales the model predictions symmetrically around zero delay. **E** Model fits (solid curves) and average subject data replotted as in Fig. 2F. The [L+M]/2 model fit is the solid curve. Other curves indicate best-fit model predictions from the S-cones (blue curve), the inner-segment diameters alone (dashed curve), and the midget ganglion cells (dotted curve).

Figure 4B plots the catch rates of the L, M, and S cones, and midget retinal ganglion cells, all relative to the foveal catches as predicted by the combined effect of the factors mentioned above. The catch rates of L-, M-, and S-cones are calculated by multiplying the spectral sensitivities of each cone type by the spectral transmittance function of the macular pigment, scaling by the influence of the inner-segment diameter and outer-segment length, and then integrating over wavelength. For purposes of comparison, we also include the catch rates for inner-segment diameters alone, and for midget retinal ganglion cells (mRGCs).[1]

To understand how the model converts catch rates into a prediction of interocular delay in each condition of our experiment, it is useful to visualize how the time required to catch the threshold

[1] The mRGC catch rate is obtained by using the number of cones in the mRGC receptive-field center at each eccentricity to scale the mean catch rate of the L- and M-cones, which implicitly assumes perfect spatio-temporal pooling. The accuracy of this assumption is challenged by findings indicating that the dynamics of the mRGCs are largely inherited from the dynamics of the cone photoreceptors themselves (Sinha et al., 2017; Baylor & Hodgkin, 1973; Drum, 1984). The mRGC catch-rates, like the inner-segment only catch-rates, should thus be thought potentially useful benchmarks for comparison, rather than as realistic physiological possibilities.

number of photons depends on the catch rate (Fig. 4C). In the bright and dark eyes, the times to response are given by

$$t_{bright} = \frac{N_0}{r(E)} \quad (1a)$$

$$t_{dark} = \frac{N_0}{r(E)} 10^{|\Delta O|} \quad (1b)$$

where N_0 is the threshold number of photons that must be caught, $r(E)$ is the catch rate as a function of eccentricity E, and $10^{|\Delta O|}$ is the transmittance T in the dark eye that corresponds to the simulated optical density difference. At a given eccentricity, the time to response is shorter in the bright eye than in the dark eye. The model-predicted interocular delay Δt is given by this difference. And because catch rates increase with eccentricity, the model predicts shorter interocular delays at peripheral than at foveal visual locations (Fig. 4C).

Model predictions of the average human data are shown in Fig. 4DE. The primary model uses the mean catch rates of the L- and M-cones (i.e. [L+M]/2) on the assumption that luminance sensitivity drives performance. A single free parameter, the threshold number of photons N_0, is fit to data across all conditions to minimize mean absolute error. This free parameter multiplicatively scales the fits symmetrically about zero. So the data patterns that the model can account for are highly constrained. The human data is nevertheless well accounted for by the model (Fig. 4D).

Fig. 4E summarizes the patterns in the data as in Fig. 2F, for several additional models derived from the factors in Fig. 4AB. These models use the catch rates of the inner-segment diameters only, the S-cones, and the midget retinal ganglion cells (mRGCs). The [L+M]/2 model accounts for the average subject data better than all the other models, and substantially so for all but the S-cone model.

Temporal delays across a reasonable expanse of the central visual field can, to first approximation, be accounted for by a simple model grounded in retinal physiology. The close match between the modeling and psychophysical results also provides strong additional support for the consensus view that the temporal properties of retinal response drive the classic Pulfrich effect. Perhaps even more intriguingly, variations in photoreceptor dynamics across the retinal surface are widespread, and occur in creatures ranging from humans to flies (Burton et al., 2001; Masland, 2017; Sinha et al., 2022). Successful compensation for, or nulling of, these differences in processing speeds must occur, or rigid scenes will be seen as being non-rigid. Such perceptual errors do not typically occur. The computational challenges that the human visual system must overcome to support accurate vision are substantial. Similar computational challenges are likely faced by visual systems across the animal kingdom.

Methods

Participants

Two male and three female subjects between the ages of 19 and 44 participated in the experiment. One male and one female subjects were authors; the other subjects were naïve to the purposes of the experiment. Visual acuity was normal or corrected-to-normal (i.e. visual acuity of 20/20 or better) in both eyes of each subject. Stereo-acuity was also normal, as assessed with the Titmus stereo test (i.e. stereoacuity better than or equal to 30arcmin). The experimental protocols were approved by the Institutional Review Board at the University of Pennsylvania and were in compliance with the Declaration of Helsinki. All participants provided written informed consent.

Apparatus

Stimuli were presented on a four-mirror haploscope. Left- and right-eye images were presented on two identical VPixx VIEWPixx LED monitors. Monitors were calibrated (i.e., the gamma functions were linearized) using custom software routines. The monitors had a size of 53.3x30.0cm, a spatial resolution of 1920x1080 pixels, a native refresh rate of 120Hz, and a maximum luminance of 105.9cd/m2. After light loss due to mirror reflections, the maximum luminance was 93.9cd/m2. The two monitors were controlled by the same AMD FirePro D500 graphics card with 3GB GDDR5 VRAM, ensuring that the left and right eye images were presented synchronously. Custom firmware was written so that each monitor was driven by a single color-channel; the red channel drove the left monitor and the green channel drove the right monitor. The single-channel drive to each monitor was then replicated in all three color channels to enable gray scale presentation.

Subjects viewed stimuli on the monitors through mirror cubes with 2.5cm circular openings positioned one inter-ocular distance apart. The field of view was approximately ±10deg. The haploscope mirrors were adjusted such that the vergence distance matched the distance travelled by the light from the monitors to the eyes. The light travelled 100cm to the eyes, a distance confirmed both by laser ruler measurements and by binocular visual comparisons with a real target at 100cm. At this distance, each pixel subtended 0.93arcmin. Stimulus presentation was controlled via the Psychophysics Toolbox-3. Anti-aliasing enabled sub-pixel resolution permitting accurate presentations of disparities as small as 15-20arcsec. The head was stabilized with a chin and forehead rest.

Stimuli

The target stimulus was a set of eight, equally-spaced circular beads that moved on one of five concentric circular paths. Each circular path was centered on a fixation point. The left- and right-eye onscreen x- and y-positions of an individual circular bead were given by

$$x_L(t) = E\cos(2\pi\omega(t + \Delta t) + \phi_i), \qquad x_R(t) = E\cos(2\pi\omega(t) + \phi_i) \qquad \text{(Xa)}$$

$$y_L(t) = E\sin(2\pi\omega(t + \Delta t) + \phi_i), \qquad y_R(t) = E\sin(2\pi\omega(t) + \phi_i) \qquad \text{(Xb)}$$

where E is the circular path's radius (i.e. the retinal eccentricity), ω is the temporal frequency of the target movement, ϕ_i is the starting phase, t is time in seconds, and Δt is the onscreen delay between the left- and right-eye target images. The circular paths had radii of 0.5, 1.0, 2.0, 4.0, and 6.0 deg of visual angle. The temporal frequency always equalled $\pm 1/\pi$ revolutions per second, so the beads moved either clockwise or anti-clockwise at constant speeds of 1.0, 2.0, 4.0, 8.0, or 12 deg/sec, depending on the eccentricity. The starting phase of the first bead of eight was chosen randomly on the interval 0 to 2π (polar angle = 360deg). The other seven beads had equally spaced starting phases separated by $\pi/4$ (polar angle = 45deg). Trial duration was 0.25 seconds.

In the original experiment, the size of the beads increased in proportion to the eccentricity (i.e. radius) of the corresponding circular path (just as did the speeds). The circular beads had diameters of 10arcmin, 20arcmin, 40arcmin, 80arcmin, and 120arcmin at five eccentricities: 0.5º, 1.0º, 2.0º, 4.0º, and 6.0º.

In the size-control experiment (see below), the bead size was fixed to 20arcmin at all of the four probed eccentricities: 1.0º, 2.0º, 4.0º, and 6.0º. We did not use the smallest bead size from the main experiment (10arcmin) because it was hard to see at large eccentricities, and we did not

probe the smallest eccentricity from the main experiment (0.5º) because 20 arcmin beads overlapped one another at the bead spacing used in the control experiment.

The onscreen interocular delay (negative or positive) and the direction of motion (clockwise or anti-clockwise) jointly determined whether onscreen stereo information specified whether the circular path was rotated 'top back' or 'bottom back' with respect to the screen. When the onscreen delay was negative, the left-eye stimulus was delayed onscreen relative to the right eye stimulus. When the onscreen delay was positive, the left eye stimulus was advanced onscreen. For clockwise motion, negative onscreen delays specified that the path was rotated 'top back' with respect to the screen and positive onscreen delays specified that the path was rotated 'bottom back' with respect to the screen. For anti-clockwise motion, the reverse was true. Note that we did not temporally manipulate when left- and right-eye images were presented onscreen. Rather, we calculated the effective binocular disparity given the target velocity and the desired onscreen delay on each time step, appropriately shifted the spatial positions of the left- and right-eye images to create an equivalent onscreen disparity, and presented these disparate images synchronously on each monitor refresh.

The onscreen interocular delay Δt can thus be equivalently expressed as a maximum onscreen disparity. The maximum onscreen horizontal disparity occurs at the top and the bottom of the circular path, where the horizontal component of the onscreen velocity is highest. At these locations, the horizontal component of the velocity v_x equals $2E\pi\omega$, the onscreen disparity in degrees of visual angle is given by

$$\delta_x = \Delta x = v_x \Delta t$$

In this paper, uncrossed disparities are negative and crossed disparities are positive. Uncrossed and crossed disparities specify distances farther and closer than the screen, respectively.

Throughout the experiments, subjects fixated a white fixation dot in the center of the screen. The fixation dot was on top of a frontoparallel disk textured with 1/f noise. The diameter of the 1/f-textured disk equalled the diameter of circular path minus the diameter of the circular bead. The periphery of the display was also textured with 1/f noise, and had an opening with a diameter that equalled the diameter of the circular path plus the diameter of the circular bead. The space between the edge of the textured disk and the edge of the textured periphery thus had a width of twice the bead diameters and served as a 'race track' that the circular beads travelled along. Both the 1/f-textured disk and 1/f-textured screen periphery aided binocular fusion and served as stereoscopic references to the screen distance. Experiments were programmed in Matlab (Matlab 2017a; Mathworks, Inc.) and presented via PsychToolbox3 (Brainard, 1997).

Procedure

Each set of moving circular beads was presented as part of a one-interval two-alternative forced-choice (2AFC) procedure. The task was to report, via a keypress, whether the circular path upon which the beads were traveling was rotated 'top back' or 'bottom back' with respect to the plane of the screen. Seven evenly spaced levels of onscreen interocular delay were presented with the method of constant stimuli. The particular levels of delay were set specifically for each subject in each condition based on pilot data.

The 'top back' and 'bottom back' responses were recorded as a function of motion direction (i.e. counter-clockwise and clockwise), onscreen interocular delay, interocular image difference, and retinal eccentricity. After appropriately collapsing across motion direction in each condition, we plotted the proportion of times subjects chose 'top-back' as a function of onscreen interocular

delay, and then fit this data with a cumulative gaussian using maximum likelihood methods. The mean of the fitted psychometric function--that is, the onscreen delay that produced 'top-back' responses 50% of the time—is the estimated point of subjective equality (PSE).The point of subjective equality (PSE) is the onscreen interocular delay necessary to make the circular beads appear to move within the screen plane. The PSE is equal in magnitude and opposite in sign to the neural delay between the eyes.

The experiment examined how luminance differences between the eyes impacted temporal processing as a function of retinal eccentricity. At each eccentricity, data was collected for each of four luminance differences. Either the left eye was delivered 75% or 50% less light than the right eye, or the right eye was delivered 50% or 75% less light than the left eye. Light losses of 75% and 50% correspond to (virtual) transmittances T of 0.25 and 0.50. The transmittance can be expressed in terms of an optical density $T = 10^{-OD}$ where OD is the optical density of a 'virtual' neutral density filter. The virtual neutral density filter is implemented by reducing the luminance of the onscreen image by a scale factor equal to the transmittance T. We express the differences in light loss between the eyes in terms of the corresponding optical density differences between the eyes $\Delta O = OD_R - OD_L$ where OD_L and OD_R are the corresponding optical densities in the left and right eyes, respectively. The luminance differences above correspond to optical density differences of ΔO=[-0.6,-0.3,+0.3,+0.6].

Data was collected at each eccentricity with all luminance difference conditions, all levels of interocular delay, and both motion directions interleaved in each of five blocks of 168 trials each (4 interocular image differences x 7 levels x 6 trials per level) for a total of 30 trials per level. Blocks probing different eccentricities were collected in pseudo-random counterbalanced order. Each block took approximately 3.5 minutes to complete. In total, at each eccentricity we collected a total 840 trials from each subject (210 trials per luminance difference x 4 luminance differences). In the main experiment, data was collected at five eccentricities (4200 trials per subject). In the size-control experiment (see below), data was collected at four eccentricities (3360 trials per subject).

Size control experiment

To determine whether stimulus bead-size impacts processing delay, we compared the critical onscreen delays from the size-control experiments against the critical onscreen delays from the original experiment. To isolate the effect of eccentricity on the data, we regressed out the mean effect in each luminance difference condition. Then we used Deming regression, which takes into account the fact that both the original and size-control estimates of critical onscreen delay are uncertain due to measurement error.

References

Bair, W., Cavanaugh, J. R., & Movshon, J. A. (2003). Time course and time-distance relationships for surround suppression in macaque V1 neurons. *Journal of Neuroscience*, *23*(20), 7690–7701.

Banks, M. S., Sekuler, A. B., & Anderson, S. J. (1991). Peripheral spatial vision: limits imposed by optics, photoreceptors, and receptor pooling. *Journal of the Optical Society of America. a, Optics and Image Science*, *8*(11), 1775–1787.

Baudin, J., Angueyra, J. M., Sinha, R., & Rieke, F. (2019). S-cone photoreceptors in the primate retina are functionally distinct from L and M cones. *Elife*, *8*, e39166.

Baylor, D. A., & Hodgkin, A. L. (1973). Detection and resolution of visual stimuli by turtle photoreceptors. The Journal of Physiology, 234(1), 163–198. http://doi.org/10.1113/jphysiol.1973.sp010340

Bolz, J., Rosner, G., & Wässle, H. (1982). Response latency of brisk-sustained (X) and brisk-transient (Y) cells in the cat retina. *The Journal of Physiology*, *328*, 171–190. http://doi.org/10.1113/jphysiol.1982.sp014258

Brainard, D. H. (1997). The Psychophysics Toolbox. *Spatial Vision*, *10*(4), 433–436.

Burge, J., & Cormack, L. K. (2020). Target tracking reveals the time course of visual processing with millisecond-scale precision. *bioRxiv*. http://doi.org/10.1101/2020.08.05.238642

Burge, J., Rodriguez-Lopez, V., & Dorronsoro, C. (2019). Monovision and the Misperception of Motion. *Current Biology*, *29*(15), 2586–2592.e4. http://doi.org/10.1016/j.cub.2019.06.070

Burton, B. G., Tatler, B. W., & Laughlin, S. B. (2001). Variations in photoreceptor response dynamics across the fly retina. *Journal of Neurophysiology*, *86*(2), 950–960. http://doi.org/10.1152/jn.2001.86.2.950

Burge, J., & Burge, T. (2023). Shape, perspective, and what is and is not perceived: Comment on Morales, Bax, and Firestone (2020). *Psychological Review*, *130*(4), 1125–1136. http://doi.org/10.1037/rev0000363

Burton, B. G., Tatler, B. W., & Laughlin, S. B. (2001). Variations in photoreceptor response dynamics across the fly retina. *Journal of Neurophysiology*, *86*(2), 950–960. http://doi.org/10.1152/jn.2001.86.2.950

Carrasco, M., McElree, B., Denisova, K., & Giordano, A. M. (2003). Speed of visual processing increases with eccentricity. *Nature Neuroscience*, *6*(7), 699–700. http://doi.org/10.1038/nn1079

Chin, B. M., & Burge, J. (2022). Perceptual consequences of interocular differences in the duration of temporal integration. *Journal of Vision*, *22*(12), 12. http://doi.org/10.1167/jov.22.12.12

Churan, J., Richard, A. G., & Pack, C. C. (2009). Interaction of spatial and temporal factors in psychophysical estimates of surround suppression. *Journal of Vision*, *9*(4), 15.1–15. http://doi.org/10.1167/9.4.15

Cottaris, N. P., & De Valois, R. L. (1998). Temporal dynamics of chromatic tuning in macaque primary visual cortex. *Nature*, *395*(6705), 896-900.

Cottaris, N. P., Jiang, H., Ding, X., Wandell, B. A., & Brainard, D. H. (2019). A computational-observer model of spatial contrast sensitivity: Effects of wave-front-based optics, cone-mosaic structure, and inference engine. *Journal of Vision*, *19*(4), 8. http://doi.org/10.1167/19.4.8

Curcio, C. A., Sloan, K. R., Kalina, R. E., & Hendrickson, A. E. (1990). Human photoreceptor topography. *Journal of Comparative Neurology*, *292*(4), 497–523. http://doi.org/10.1002/cne.902920402

Dacey, D., Packer, O. S., Diller, L., Brainard, D., Peterson, B., & Lee, B. (2000). Center surround receptive field structure of cone bipolar cells in primate retina. *Vision Research*, *40*(14), 1801–1811.

Drum, B. (1984). Cone response latency and log sensitivity: proportional changes with light adaptation. Vision Research, 24(4), 323–331. http://doi.org/10.1016/0042-6989(84)90057-9

Harwerth, R. S., & Levi, D. M. (1978). Reaction time as a measure of suprathreshold grating detection. *Vision Research*, *18*(11), 1579–1586. http://doi.org/10.1016/0042-6989(78)90014-7

Jovanovic, L., & Mamassian, P. (2020). Events are perceived earlier in peripheral vision. *Current Biology*, *30*(21), R1299–R1300. http://doi.org/10.1016/j.cub.2020.08.096

Kelly, D. H. (1984). Retinal inhomogeneity. I. Spatiotemporal contrast sensitivity. *Journal of the Optical Society of America. a, Optics and Image Science*, *1*(1), 107–113. http://doi.org/10.1364/josaa.1.000107

Lennie, P. (1981). The physiological basis of variations in visual latency. *Vision Research*, *21*(6), 815–824. http://doi.org/10.1016/0042-6989(81)90180-2

Lit, A. (1949). The magnitude of the Pulfrich stereophenomenon as a function of binocular differences of intensity at various levels of illumination. The American Journal of Psychology, 62(2), 159–181.

Mansfield, R. J., & Daugman, J. G. (1978). Retinal mechanisms of visual latency. *Vision Research*, *18*(9), 1247–1260. http://doi.org/10.1016/0042-6989(78)90111-6

Masland, R. H. (2017). Vision: Two Speeds in the Retina. *Current Biology*, *27*(8), R303–R305. http://doi.org/10.1016/j.cub.2017.02.056

Min, S. H., Reynaud, A., & Hess, R. F. (2020). Interocular Differences in Spatial Frequency Influence the Pulfrich Effect. *Vision*, *4*(20), 1–13. http://doi.org/10.3390/vision4010020

Nachmias, J. (1967). Effect of Exposure Duration on Visual Contrast Sensitivity with Square-Wave Gratings. *Journal of the Optical Society of America*, *57*(3), 421–427.

Pulfrich, C. (1922). Die Stereoskopie im Dienste der isochromen und heterochromen Photometrie. *Die Naturwissenschaften*, *10*(35), 553–564.

Reynaud, A., & Hess, R. F. (2017). Interocular contrast difference drives illusory 3D percept. *Scientific Reports*, *7*(1), 5587. http://doi.org/10.1038/s41598-017-06151-w

Rodriguez-Lopez, V., Dorronsoro, C., & Burge, J. (2020). Contact lenses, the reverse Pulfrich effect, and anti-Pulfrich monovision corrections. *Scientific Reports*, *10*, 1–16. http://doi.org/10.1038/s41598-020-71395-y

Rodriguez-Lopez V, Chin BM, Burge J (2023). The effect of overall light-level on the reverse Pulfrich effect. *bioRxiv*, 559782, 1-17.

Rogers, B. J., & Anstis, S. M. (1972). Intensity versus adaptation and the Pulfrich stereophenomenon. *Vision Research*, *12*(5), 909–928.

Prestrude, A. M., & Baker, H. D. (1968). New method of measuring visual-perceptual latency differences. *Perception & Psychophysics*, *4*, 152–154.

Prestrude, A. M. (1971). Visual Latencies at Photopic Levels of Retinal Illuminance. *Vision Research*, *11*(4), 351–. http://doi.org/10.1016/0042-6989(71)90246-X

Sinha, R., Hoon, M., Baudin, J., Okawa, H., Wong, R. O. L., & Rieke, F. (2017). Cellular and Circuit Mechanisms Shaping the Perceptual Properties of the Primate Fovea. *Cell*, *168*(3), 413–426.e12. http://doi.org/10.1016/j.cell.2017.01.005

Sinha, R. (2022). Light adaptation in primate fovea (Vol. 22, pp. 44–44). Presented at the Optica Fall Vision Meeting.

Virsu, V., Rovamo, J., Laurinen, P., & Nasanen, R. (1982). Temporal contrast sensitivity and cortical magnification. *Vision Research*, *22*(9), 1211–1217. http://doi.org/10.1016/0042-6989(82)90087-6

Watson, A. (1986). Temporal sensitivity. In K. Boff, J. Thomas, & L. Kaufman (Eds.), (Vol. 1). Handbook of perception and human performance.

Wolpert, D. M., Miall, R. C., Cumming, B., & Boniface, S. J. (1993). Retinal adaptation of visual processing time delays. *Vision Research*, *33*(10), 1421–1430.

Supplement

Eccentricity strongly modulates visual processing delays

Johannes Burge[1,2,3,*] & Callista M. Dyer[1]

[1.]Department of Psychology, University of Pennsylvania, Pennsylvania PA
[2.]Neuroscience Graduate Group, University of Pennsylvania, Pennsylvania PA
[3.]Bioengineering Graduate Group, University of Pennsylvania, Pennsylvania PA
[*]Correspondence to jburge@upenn.edu

All individual subject data: Original and size-control experiment
Delay discrimination thresholds are shown for all five human subjects (Fig. S1AB). For each observer, discrimination thresholds decrease with eccentricity. This result is consistent with an increase in temporal contrast sensitivity—which is well-known to improve in the peripheral visual field (Kelly, 1984). Also interestingly, like the critical onscreen delays, the delay discrimination thresholds are also reasonably well characterized by power functions, which plot as straight lines on log-log plots (Fig. S1B).

All five human subjects showed approximately the same pattern of critical onscreen delays in the main experiment and in the size-control experiment, and approximately matches the average human data (Fig. S2A-C; also see Figs. 2,3). Four of the five subjects produced data that was clean enough to evaluate whether the effect of eccentricity in the original and size-control experiments was the same. For each of these four human subjects, the effect of eccentricity in each luminance difference condition is significantly correlated, and the best-fit regression lines to this data have slopes that were not significantly different 1.0. Data from the fifth subject is too noisy to draw firm conclusions (Fig. S2D). In general, the size-control experiment shows that there is no reason to think that bead-size, rather than eccentricity, drove the pattern of visual processing delays.

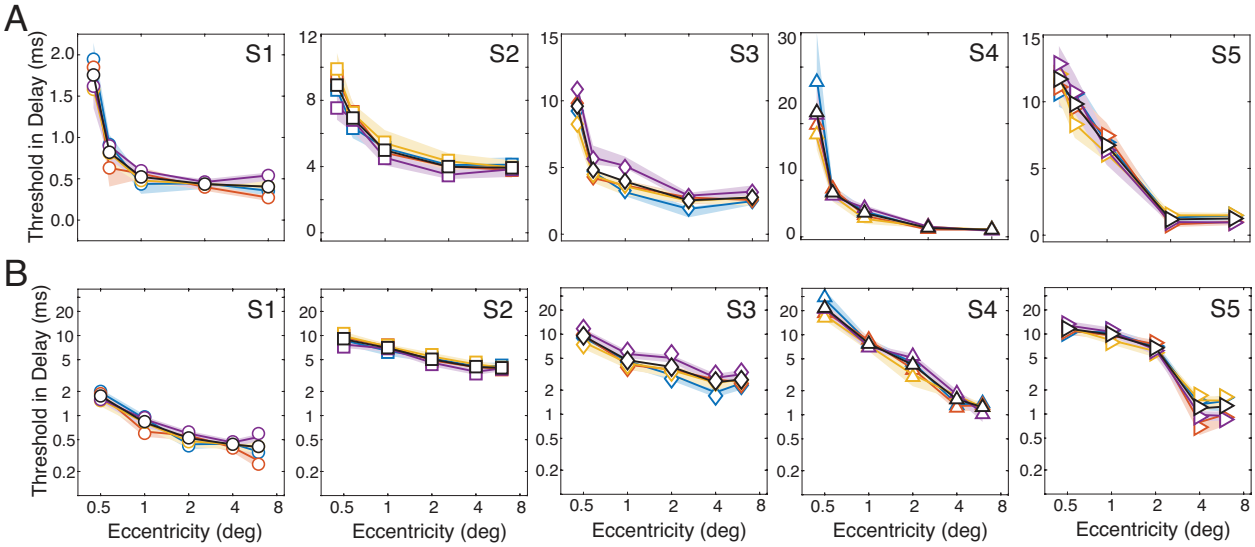

Figure S1. Individual subject thresholds in delays. **A** Thresholds on linear-linear axes. Note that the y-axis range is different for each subject. **B** Thresholds on log-log axes. The data is reasonably approximated by straight lines on the log-log plots indicating that— like the critical onscreen delays—a power function well-describes the change with eccentricity.

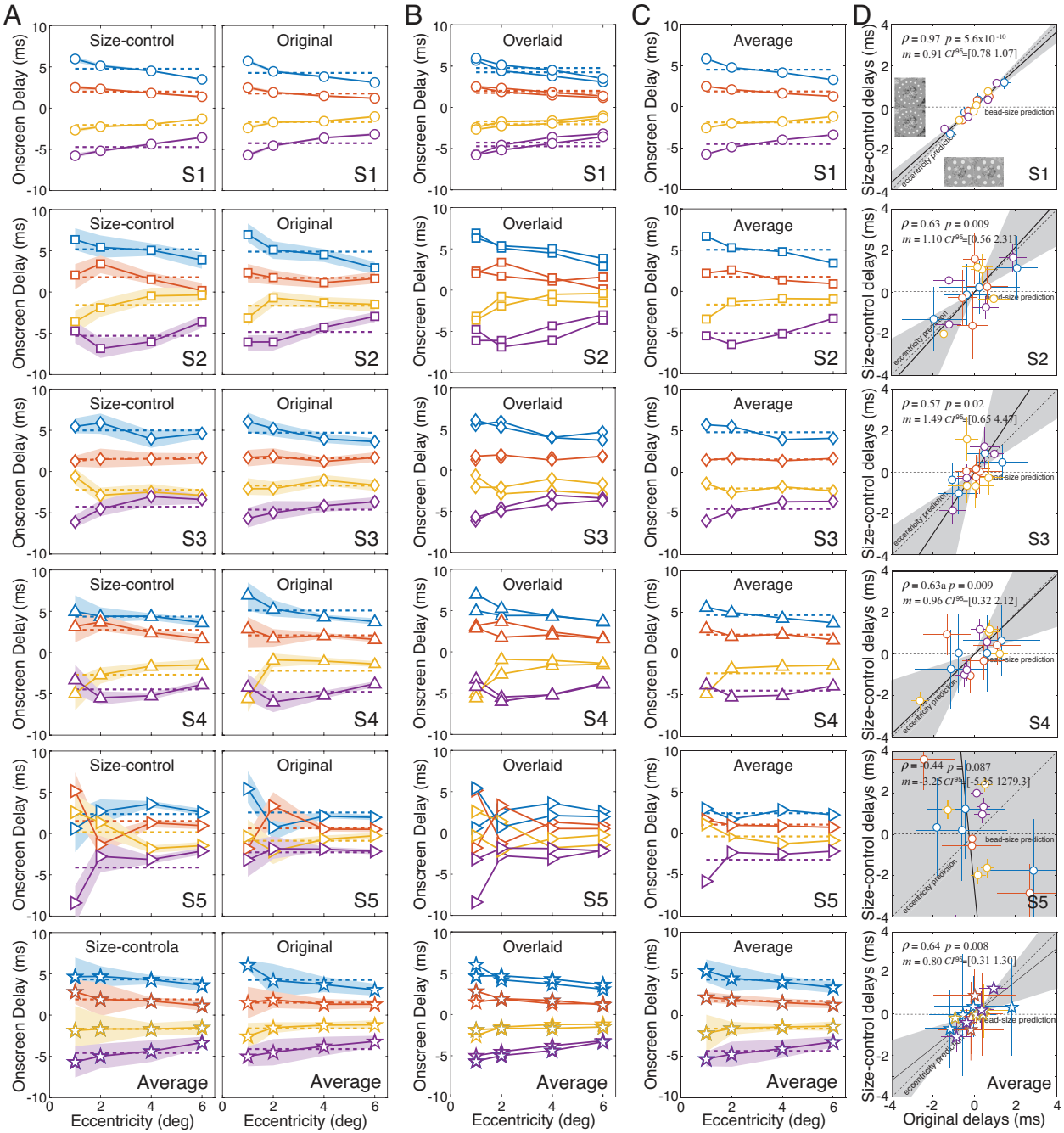

Figure S2. Individual subject, and average, data in original and size-control experiments. **A** Critical onscreen delays as a function of eccentricity at each luminance difference (colors) in both the control experiment (left) and the original experiment (right) for all five human subjects. Dashed lines indicate the mean delay at each luminance condition (colors). Each row contains the data for a different subject. **B** Overlaid data from A. **C** Critical onscreen delays averaged across the original and control experiments for each luminance difference and eccentricity. **D** Comparison of the effect of eccentricity in the original and size-control experiments, after regressing out the effect of luminance difference. The effect of eccentricity is significantly correlated in four of the five subjects, with best-fit slopes that are not significantly different from the unity line.